# A SCALED BOUNDARY MULTISCALE APPROACH TO CRACK PROPAGATION

**ADRIAN W. EGGER**[*], **SAVVAS P. TRIANTAFYLLOU**[†] **AND ELENI N. CHATZI**[*]

[*]Swiss Federal Institute of Technology Zurich (ETHZ)
Zurich, Switzerland
e-mail: egger@ibk.baug.ethz.ch and chatzi@ibk.baug.ethz.ch

[†]University of Nottingham
Nottingham, UK
e-mail: savvas.triantafyllou@nottingham.ac.uk

**Key words:** Linear Elastic Fracture Mechanics (LEFM), Crack Propagation, Scaled Boundary Finite Element Method (SBFEM), Extended Multiscale Finite Element Method (EMsFEM)

**Abstract.** In this work, we fuse the scaled boundary finite element method (SBFEM) on balanced hybrid quadtree-polygon (QT) meshes with the extended multiscale finite element method (EMsFEM) to accelerate crack propagation simulations. This scaled boundary multiscale approach to crack propagation employs SBFEM in a fully resolved region immediately surrounding the crack tip and coarse elements, i.e., EMsFEM unit cells, in the remaining domain. As the crack propagates across the domain, unit cells within the immediate crack path are resolved. Once the crack completely transitions a resolved unit cell it is replaced by two newly constructed, coarse unit cells. This approach limits computational effort to the crack tip region, primarily replacing the fine mesh on the domain by a coarse one, on which the governing equations are solved. Early results indicate that this method results in a reduction of required degrees of freedom (DOFs) by at least an order of magnitude for simple domains. Further techniques, unique to the SBFEM, are exploited to enrich the crack tip element and further reduce the amount of refinement necessary about the crack tip. The latter traditionally negatively affects the QT mesh due to the balancing operation. Via fusion of these two techniques, the amount of DOFs during simulations of crack propagation remains tractable.

## 1 INTRODUCTION

The demand for sustainable design in, e.g. the aerospace, automotive and construction industries has lead to the development of lighter, stronger and more resilient structures, spawning the need to guard against failure processes by leveraging robust, economical and high-fidelity numerical simulations.

The finite element method (FEM) comprises the numerical method of choice in the industry, due to its advanced level of maturity. However, many challenges characterizing singularities and propagating discontinuities remain for numerical methods that rely on a discrete crack representation:

1. A conforming mesh topology is required
2. Polynomial-based interpolation functions cannot reproduce the singular stress field
3. Algorithmic challenges in tracking crack paths, incorporating branching and merging behaviour
4. Mesh dependant projection errors may arise during nonlinear and dynamic analyses

1

5. No uniform and theoretically sound treatment of nucleation, branching and merging of cracks currently available

6. Special post-processing methods to extract the stress intensity factors (SIFs)

The extended finite element method (XFEM), proposed by Moës [10] and widely adopted in industry and academia alike, mitigates many of the above issues related to mesh dependency and treatment of singularities by locally enriching the finite element approximation space with known features of the solution. A less known alternative, namely the scaled boundary finite element method (SBFEM) [25], does not require a priori knowledge of the singularity, since its analytic solution in radial direction naturally incorporates the singular stress field and permits elegant and efficient extraction of the generalized stress intensity factors (gSIFs) during post-processing without the need for special post-processing tools.

SBFEM distinguishes itself from other numerical methods by the introduction of a scaling center in each element and a resulting semi-analytic formulation. This key concept was first adopted in other engineering fields, e.g., the solution of electric field problems [21]. Within the context of solid mechanics, Dasgupta et al. [4] first applied this approach and named it the "cloning algorithm". A similar formulation was subsequently adopted by Wolf and Song [33], who standardized a derivation by minimal weighted residual method [32,34] they then called "SBFEM". Although originally developed to tackle problems of unbounded domains, highly encouraging results were obtained for bounded domains [32], particularly within the context of LEFM [3,24]. SBFEM's analytic solution in radial direction, which enables the robust transition between power and power-logarithmic singularities [24] permitted the investigation of various multi-material scenarios without a priori knowledge of the order of singularity. Hence, multi-material plates under both static and dynamic loading [23] as well as the crack propagation direction at bi-material

notches [11] have been studied. SBFEM was first extended to modelling crack propagation problems by Yang et al. [35]. The initial meshes were created manually, employing few large sized subdomains. Subsequent extensions permitted the treatment of crack propagation in reinforced concrete [17], under dynamic excitation [18, 19] and a nonlinear cohesive fracture model in concrete [13, 36, 37]. However, the limitation of this laborious meshing approach sparked research into the adoption of newly developed polygon mesh generators [16, 28], which enabled fully automatic modelling of crack propagation employing SBFEM as the underlying discretization method. However, since the construction of the SBFEM stiffness matrix requires the solution of an eigenproblem, use of polygonal elements incurred significant computational cost. This was alleviated with the advent of quadtree based meshers in conjunction with polygon clipping, in order to accurately represent domains not aligned with a Cartesian grid [12], even at coarse discretization levels. The balancing approach introduces 16 possible element realization, which are pre-computed and retrieved as necessary, such that the main source of computational effort stems from the construction of the stiffness matrices for clipped polygons on the boundary. While SBFEM significantly accelerates LEFM-related computations [7], the simulation of more involved problems bridging multiple scales still poses a considerable challenge. One possible way to mitigate such issues is by utilizing multiscale methods.

To this end, several numerical homogenization methods have been proposed [6]. Here we utilize the extended multiscale finite element method (EMsFEM) [40], which applies the FEM to compute the homogenized material parameters and map the microscopic response to the macroscopic system response. The central idea is to numerically construct this mapping by locally solving a series of Dirichlet boundary value problems. Its predecessor, MsFEM, was first applied to two-phase flow and transport problems in highly heterogenous

porous media [8]. An augmentation thereof, the coupling MsFEM, treated the consolidation of heterogeneous saturated porous media [38]. The further inclusion of Poisson's effect in construction of the mapping led to its applicability in computational solid mechanics [39, 40] and labelling as EMsFEM. Triantafyllou and Chatzi subsequently proposed the hysteretic multiscale finite element method (HMsFEM) [29], which treats nonlinear static and dynamic analysis of heterogeneous structures within the hysteretic finite element framework [31]. The multi-axial smooth hysteretic model controlling the evolution of plastic strains follows the Bouc-Wen model of hysteresis [1]. This approach was later applied to model validation in reliability analysis and inverse problem formulations [30].

The aim of this work is to fuse existing SBFEM based approaches, augmented by a newly proposed method to locally enhance the accuracy of gSIFs, with established EMsFEM principles, enabling efficient crack propagation simulations for large systems. By minimizing and stabilizing the amount of DOF required during analysis, computational effort and thus computation times are kept stable, enabling the analysis of previously intractable systems.

The remaining sections of this paper are structured as follows: Sec. 2 presents the pertinent theory. In sec. 3 the proposed method is detailed. Numerical examples are solved in sec. 4 and conclusions are drawn in sec. 5.

## 2 THEORY

### 2.1 Problem Statement

In formulating the LEFM problem, we consider a two dimensional cracked domain $\Omega$. The boundary $\Gamma$ consists of $\Gamma_0$ with free surface boundary conditions, $\Gamma_u$ with prescribed displacements $\bar{u}$ and $\Gamma_t$ with surface tractions $\bar{t}$ applied as Neumann conditions. Free surface conditions apply to the crack surface $\Gamma_c$. As depicted in Fig. 1, the whole boundary of the body comprises $\Gamma = \Gamma_0 \cup \Gamma_u \cup \Gamma_t \cup \Gamma_c$ . The strong form with boundary conditions is stated as:
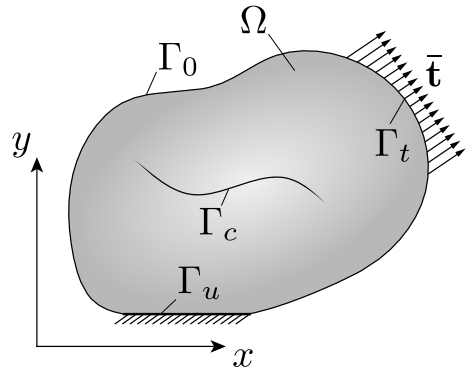


Figure 1: Cracked Body and boundary conditions.

$$
\begin{aligned}
\nabla \cdot \sigma + b &= 0 && \text{in} && \Omega && \text{(1a)} \\
u &= \bar{u} && \text{on} && \Gamma_u && \text{(1b)} \\
\sigma \cdot n &= \bar{t} && \text{on} && \Gamma_t && \text{(1c)} \\
\sigma \cdot n &= 0 && \text{on} && \Gamma_c^0 && \text{(1d)} \\
\sigma \cdot n &= \bar{t}_c && \text{on} && \Gamma_c^t && \text{(1e)}
\end{aligned}
$$

where the Cauchy stress tensor, unit outward normal to the boundary, applied body force per unit volume, displacement field and gradient operator are denoted as $\sigma$, $n$, $b$, $u$ and $\nabla$ respectively.

Within the context of LEFM the material is defined by the modulus of elasticity $E$ and Poisson ratio $\nu$, thus the strain field $\epsilon$ and the stress field $\sigma$ follow as:

$$
\epsilon = \nabla_s u \quad \text{and} \quad \sigma = D\epsilon \tag{2}
$$

where $\nabla_s$ refers to the symmetric gradient operator and in 2D $[D]$ is the elasticity tensor.

### 2.2 Summary of SBFEM Theory

The distinguishing feature of SBFEM [25] is the introduction of a scaling center. One scaling center, from which the entire boundary must be visible, is present in each polygonal SBFEM element, termed a subdomain. Consequently, the transition in reference system from Cartesian to one resembling polar coordinates introduces the radial coordinate $\xi$ and local tangential coordinate $\eta$ (Fig. 2). The radial coordinate takes on the values $\xi = 0$ at the scaling center and $\xi = 1$ on the boundary. Keeping this component analytic during the entire analysis permits the reduction in dimensionality of the problem by one. For the case of

2D bounded domains, it follows that only discretization of the subdomain's boundary, in the finite element sense, into independent line elements is required. Standard line elements are employed, each with a separate local coordinate $\eta$ spanning $-1 < \eta < 1$.
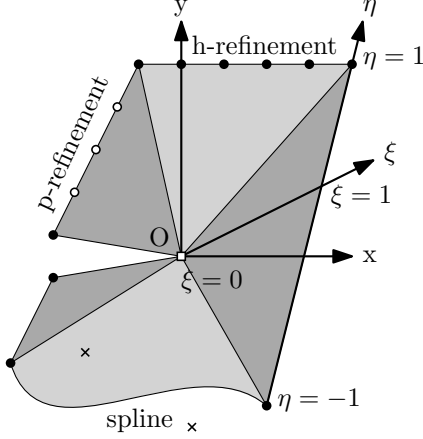


Figure 2: Subdomain with scaled boundary coordinates $\xi$ and $\eta$.

The mapping between Cartesian $(x, y)$ and scaled boundary coordinates $(x(\xi, \eta), y(\xi, \eta))$ results from scaling any point $(x_b, y_b)$ that sits on the boundary along the radial component $\xi$, while employing conventional finite element shape functions $[N(\eta)]$ in tangential direction. This mapping is expressed as follows:

$$x(\xi, \eta) = \xi x_b(\eta) = \xi[N(\eta)]\{x_b\} \quad (3)$$
$$y(\xi, \eta) = \xi y_b(\eta) = \xi[N(\eta)]\{y_b\} \quad (4)$$

Similarly the displacements contain an analytic, $\{u(\xi)\}$, and interpolatory, $[N(\eta)]$, component:

$$\{u(\xi, \eta)\} = [N_1(\eta)[I], ..., N_n(\eta)[I]]\{u(\xi)\} \quad (5)$$

The amount of degrees of freedom (DOF) present in a line element is denoted by the subscript $n$. Here, $[I]$ is the $2 \times 2$ identity matrix, while $\{u(\xi)\}$ is an analytic function of the nodal displacements along the line given by $0 < \xi < 1$. It can be shown that the stresses follow as [27]:

$$\{\sigma(\xi, \eta)\} = [D]([B^1(\eta)]\{u(\xi)\},_\xi + [B^2(\eta)]\{u(\xi)\}/\xi) \quad (6)$$

The strain-displacement relation is described by the combination of $[B^1(\eta)]$ and $[B^2(\eta)]$ [25]. The governing differential equation is recast into scaled boundary coordinates, which, upon application of standard techniques along $\eta$, gives rise to two equations [5, 9, 32]:

$$[E^0]\xi^2\{u(\xi)\},_{\xi\xi} + [[E^0] + [E^1]^T - [E^1]]\xi\{u(\xi)\},_\xi$$
$$- [E^2]\{u(\xi)\} = \{0\} \quad (7)$$

$$\{P\} = [E^0]\{u_h\},_\xi + [E^1]^T\{u_h\} \quad (8)$$

Behaviour within the domain is described by Eqn. 7. Behaviour on the boundary is governed by Eqn. 8. $\{P\}$ is the nodal force vector and $\{u\} = \{u(\xi = 1)\}$. The coefficient matrices $[E^0], [E^1], [E^2]$ are treated analogousness to a stiffness matrix in the FEM: Calculated for each element individually and then assembled. This homogeneous set of Euler-Cauchy differential equations in $\xi$, has a general solution in the form of a power series:

$$\{u(\xi)\} = [\Psi^{(u)}]\xi^{-[S]}\{c\} = \sum_{i=1}^{n}[\Psi_i^{(u)}]\xi^{-[S_i]}\{c_i\} \quad (9)$$

The established solution procedure entails recasting the Eqns. 7 and 8 as a system of first order differential equations, from which the transformation matrix $[\Psi]$ and block diagonal real Schur form $[S]$ are ultimately derived:

$$\xi \begin{Bmatrix} \{u(\xi)\} \\ \{q(\xi)\} \end{Bmatrix},_\xi = -[Z] \begin{Bmatrix} \{u(\xi)\} \\ \{q(\xi)\} \end{Bmatrix} \quad (10)$$

where Z is a Hamiltonian coefficient matrix

$$Z = \begin{bmatrix} [E^0]^{-1}[E^1]^T & -[E^0]^{-1} \\ -[E^2] + [E^1][E^0]^{-1}[E^1]^T & -[E^1][E^0]^{-1} \end{bmatrix} \quad (11)$$

and the block-diagonal Schur decomposition [22] decouples Eqn. 10.

$$[Z][\Psi] = [\Psi][S] \quad (12)$$

The eigenvalues are now contained in the diagonal blocks of the real Schur form, while the columns of the transformation matrix contain the modes. The sign of the eigenvalues determines if a mode contributes to the bounded or unbounded response of the subdomain. Separating these two responses comprises sorting of $[S]$ and $[\Psi]$ with subsequent partitioning according to sign.

$$[S] = diag([S_{neg}], [S_{pos}]) \quad (13)$$

$$[\Psi] = \begin{bmatrix} [\Psi_{neg}^{(u)} & \Psi_{pos}^{(u)}] \\ [\Psi_{neg}^{(q)} & \Psi_{pos}^{(q)}] \end{bmatrix} \quad (14)$$

The stiffness matrix of the subdomain can then be derived by expressing the nodal forces on the boundary with enforced integration constants (Eqn. 9 in Eqn. 8). The displacement solution is then calculated analogous to FEM:

$$K_{bounded} = [\Psi_{pos}^{(q)}][\Psi_{neg}^{(u)}]^{-1} \qquad (15)$$

Upon substitution of Eqn. 9 into Eqn. 6 the stresses are obtrained:

$$\{\sigma(\xi,\eta)\} = \sum_{i=1}^{n}[\Psi_{\sigma i}(\eta)]\xi^{-[S_i]-[I]}\{c_i\}] \qquad (16)$$

where $[\Psi_{\sigma i}(\eta)]$, the stress mode, is linked to its corresponding displacement mode $[\Psi_i^{(u)}]$ by:

$$[\Psi_{\sigma i}(\eta)] = [D](-[B^1(\eta)][\Psi_i^{(u)}][S_i] + [B^2(\eta)][\Psi_i^{(u)}]) \qquad (17)$$

## 2.3 Generalized Stress Intensity Factors

Extraction of the gSIFs follows from inspection of the general solution to the SBFEM equation (Eqn. 9). The singular modes are readily identified by all $-1 < real(\lambda) < 0$, which can be shown to invoke a singular response at $\xi = 0$. If the scaling center coincides with the crack tip, this feature is leveraged to calculate the gSIFs (Fig. 2) by taking the limit of the singular stresses as $\xi \to 0$. The inclusion of a double node at the crack mouth gives rise to two additional modes, the singular modes, corresponding to the mode I and II fracture cases respectively. Singular quantities, i.e., the singular stress field, are retained from the general solution (Eqn. 16) and denoted by the superscript $(s)$:

$$\{\sigma^{(s)}(\xi,\eta)\} = [\Psi_\sigma^{(s)}(\eta)]\xi^{-([S^{(s)}]-[I])}\{c^{(s)}\} \qquad (18)$$

A transformation into polar coordinates is performed and the rotated components $\{\sigma^{(s)}(r,\theta)\} = (\sigma_\theta^{(s)}(r,\theta), \tau_{r\theta}^{(s)}(r,\theta))^T$ corresponding to mode I and mode II cracks are retained:

$$\begin{Bmatrix} \sigma_\theta^{(s)}(r,\theta) \\ \tau_{r\theta}^{(s)}(r,\theta) \end{Bmatrix} = \frac{1}{\sqrt{2\pi L}}\xi^{-[\tilde{S}^{(s)}(\theta)]}\begin{Bmatrix} K_I(\theta) \\ K_{II}(\theta) \end{Bmatrix} \qquad (19)$$

By comparison of Eqn. 19 to the gSIFs formal definition [26], they are evaluated as:

$$\begin{Bmatrix} K_I(\theta) \\ K_{II}(\theta) \end{Bmatrix} = \sqrt{2\pi L}\{\sigma^{(s)}\} \qquad (20)$$

## 2.4 Hierarchial Meshes

The use of quadtree decompositions to build simulation ready meshes for SBFEM analysis has enjoyed great interest in very recent literature [2, 14, 15]. Taking advantage of SBFEM's polygon underpinnings, all issues commonly associated with hanging nodes are alleviated. Further, balancing the mesh (Fig. 3b) results in only 16 precomputable subdomain orientations. Polygon clipping [12] is employed in order to incorporate strong discontinuities. Double nodes are introduced in the process and traversed subdomains are split into two accordingly. Crack tip elements comprise an additional node at the crack mouth, with the crack tip coinciding with the scaling center (Fig. 2). Crack propagation within the LEFM context requires the accurate calculation of the gSIFs in order to determine the crack propagation angle. To this end, sufficient angular resolution of the singular stress field is required. Since the precomputed elements generally do not suffice, a region around the crack tip is homogenized (Fig. 3c) by a macro crack tip element. The location of the subsequent crack tip is obtained by projecting (Fig. 3d) the existing crack tip by a user specified increment $\Delta a$ in direction of the determined crack propagation angle. Unfortunately, refinement and subsequent homogenization of the crack tip element does introduce a significant amount of additional DOF, since the balancing operation propagates across the mesh. A method to mitigate this issue is investigated at the end of the following section.

## 2.5 EMsFEM

Implementing EMsFEM comprises four steps. Quantities calculated during the first two remain constant during analysis, while the latter two are performed at each iteration.

1. Numerically construct the basis functions
2. Evaluate the equivalent coarse element stiffness matrix
3. Solve the governing equations on the macro-scale
4. Downscaling of the macro-scale solution

5
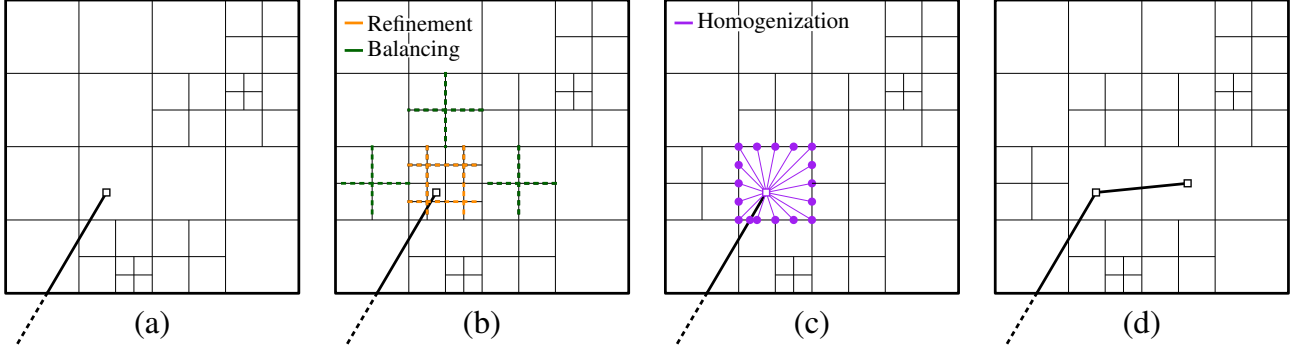
Figure 3: Introduction of SBFEM specific discretization of the domain.

The basis functions (NBF) providing the mapping between scales are constructed numerically by solving a Dirichlet boundary value problem on a unit cell. In this work, we implement linear boundary conditions. These are constructed sequentially and independently of each other. Example boundary displacements are illustrated in Fig. 4: A unit displacement is imposed at node 1 in x-direction. Displacements in x-direction vary linearly, analogous to bilinear shape functions, along the boundaries 12 and 14. The whole domain is constrained in y-direction. Additionally, boundaries 23 and 34 are further constrained in x-direction.
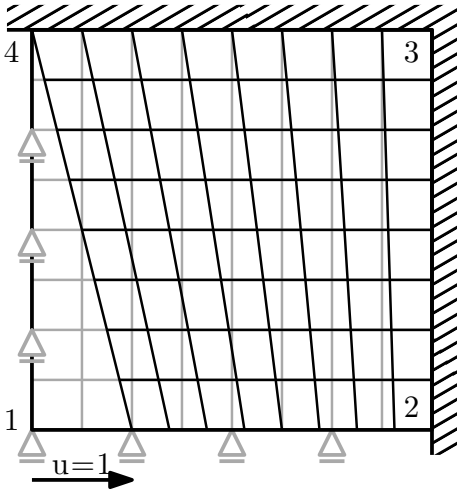


Figure 4: Construction the NBF by solving the associated Dirichlet boundary condition.

The resulting displacement solution comprises a column entry of the basis function mapping the effect of a unit displacement of the coarse scale to the response on the fine scale. Completing the procedure for all coarse DOF

results in:

$$\{u\} = [N]\{u'_E\} \tag{21}$$

where $\{u\}$ contains the displacements of the fine scale mesh, $\{u'_E\}$ is the displacement vector of the coarse mesh and [N] the basis function matrix. Here, [N] is a nDOF x 8 matrix for a unit cell of 4 coarse nodes and 2 DOF per node, with column obtained by solving the associated Dirichlet boundary value problem. The method does not impose a limit on the amount of coarse nodes permitted per unit cell. Hence coarse element representing unit cells are abbreviated as CMX, where "CM" refers to coarse multiscale elements and "X" is the amount of coarse nodes.

The equivalent stiffness matrix of a coarse element is obtained by energy equivalence. To this end, the strain energy of the fine scale is mapped to the coarse scale by means of Eqn. 21.

$$\Pi_e = \frac{1}{2}u_e^T K_e u_e = \frac{1}{2}u_E'^T N^T K_e N u_E' \tag{22}$$

with the equivalent stiffness matrix of the unit cell given as $K_E = N^T K_e N$.

The macro-scale computations are then performed in the standard FEM sense. Upon solution of the governing equations on the coarse mesh, downscaling operations are necessary to evaluate the fine scale response. Through reversing Eqn. 21 the displacements are provided for each element on the fine scale and the standard procedures for strain and stress evaluation are available.

## 3  PROPOSED METHOD

The proposed method is split into two distinct phases: online and offline calculations. The offline phase comprises the identification and precomputation of the coarse elements. The computational burden associated with the repeated solution of the Dirichlet boundary value problem is minimized by first condensing the internal DOF and then constructing $[N]$, or by decomposing the stiffness matrix by direct methods. The online phase comprises the crack propagation scheme. To this end, the unit cells in vicinity of the crack tip are fully resolved, meshed and their elements assembled in the finite element sense. In parallel, the coarse elements comprising the remaining domain are also assembled and the coarse and fine meshes are tied together by penalty method (Fig. 5, blue lines), to not introduce further DOF in the process. The linear boundary conditions employed during construction of the unit cells imply linear displacements between coarse nodes (Fig. 5, red dots), defining the tie constraint behaviour. The system is then solved for and the crack is propagated according to a prescribed crack increment $\Delta a$ and computed crack propagation angle [20]:

$$\theta_c = 2\tan^{-1}\left[\frac{-2K_I/K_{II}}{1+\sqrt{1+8(K_I/K_{II})^2}}\right] \quad (23)$$

The accurate calculation of the gSIFs is paramount. However, sufficient angular resolution of the singular stress field is required. Typically, this is achieved by homogenizing a region around the crack tip (Fig. 3c) at the expense of introducing a significant number of DOF due to the balancing requirement. This work investigates an alternate approach, which does not introduce additional DOF in the process. By inspection of Eqn. 18, the stress solution can be improved in two ways: Reduce the error of the integration constants $\{c\}$, by refining the mesh or improve the approximation space of the element by adding more eigenpairs $[\Psi]$ and $[S]$ respectively. For the latter, hp-refinement on the cracked element is performed in post-processing and boundary displacements

compatible with the surrounding mesh are imposed. Thus, the error stemming from the element's approximation space is minimized. This procedure is investigated in the first example of sec. 4. Hence, similar accuracy for the gSIFs is obtained at significantly fewer DOF, alleviating the computational burden stemming from the fully resolved subdomain.

## 4  NUMERICAL EXAMPLES

### 4.1  Edge cracked square plate in mode I

An edge cracked square plate subject to a plane stress state is examined (Fig. 6). The bottom edge of the domain is fully restrained, while a forced displacements of $u_y = 1$ and $u_x = 0$ are applied to the top edge, eliciting mode I behaviour. The material properties are $E = 200$ [N/mm$^2$], $v = 0.3$, $G_c = 2.7$ [N/mm$^2$] and the side length is $L = 1$ [mm].
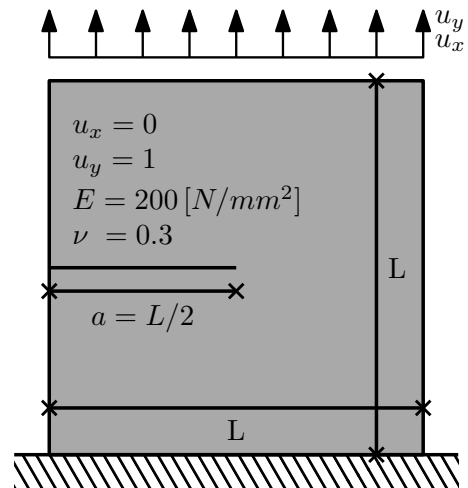


Figure 6: Experimental setup for numerical example 1.

For crack propagation a crack increment of $\Delta a = 0.025$ [mm] is imposed for each step. To this end, load-deflection curves for several methods are compared: (i) XFEM, (ii) tradtional QT SBFEM, (iii) SBFEM with crack tip elements corresponding to QT mesh types A-C (Fig. 7), (iv) the newly proposed SBFEM method and (v) a high fidelity SBFEM solution comprising one subdomain with hp-refinement.

In this first numerical example, only the benefits of enhancing the solution space of the crack tip element are assessed. Since the crack

7
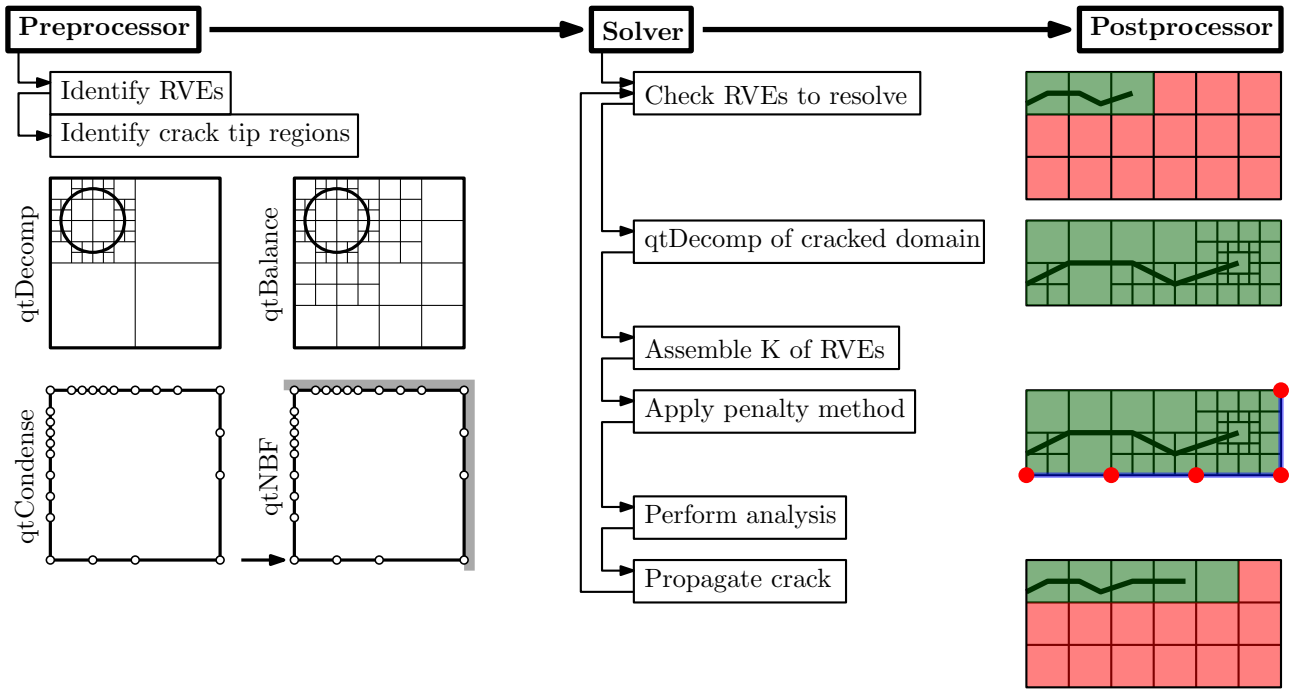
Figure 5: Scaled boundary multiscale approach to crack propagation (MSBFEM).

path for all methods overlap, i.e., they propagate in direct extension of the imposed crack, no corresponding figure is provided. The load deflection curves (Fig. 8) overlap similarly, validating the novel approach: The same amount of initial DOF are employed, i.e., 880, as for method (iii), however, the accuracy of the traditional approach (ii) utilizing 1024 initial DOF is achieved. Method (iii) is an example of insufficient angular resolution of the singular stress, which results in an oscillatory crack path due to inaccurately calculated gSIFs.
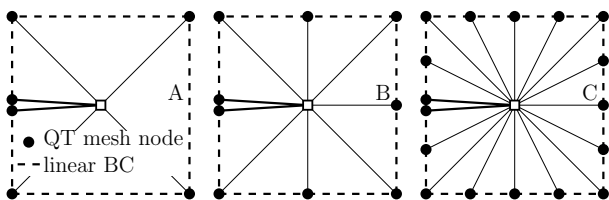


Figure 7: Typical element types A-C arising from QT meshes.

As the crack reaches the right domain edge, the traditional approach accumulates 6150 DOF, since it updates the mesh from the previous iteration, while the proposed method counts 942 DOF, since it updates the mesh from the original configuration. The reduction in

DOF is achieved by alleviating the need for refinement around the crack tip at each step, which by virtue of the balancing operation performed on the QT mesh can effect the entire domain. Further, the obtained results coincide with those obtained from a fine XFEM analysis (i) employing a domain discretization of 161x161 element and a high fidelity SBFEM solution (v) employing 568 DOF.
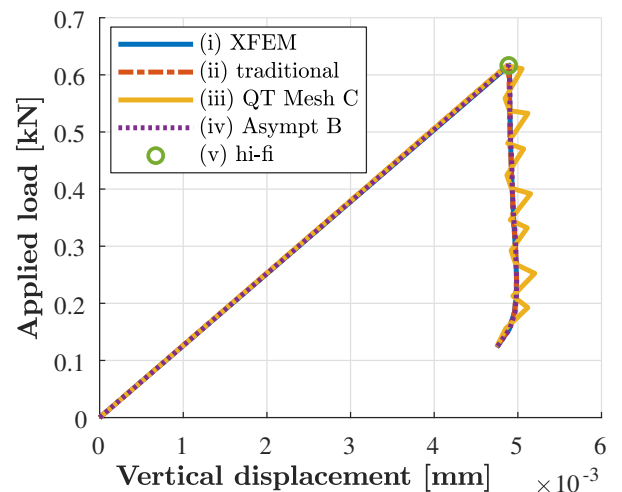


Figure 8: Load deflection curves for methods (i) - (v).

The exact solution for this type of domain

mandates a square root singularity, which states that all eigenvalues contained in $[S^{(s)}]$ (Eqn.18) equal 0.5. This property is purely a reflection of the quality of the element's approximation space. Tab. 1 tallies the results for the SBFEM based methods.

Table 1: Convergence of eigenvalues to square root singularity.

| Method | | nDOF | $\lambda_1$ | $\lambda_2$ |
|---|---|---|---|---|
| exact | | - | 0.5 | 0.5 |
| (ii) trad. | 2 | 34 | 0.5021064963 | 0.5021064963 |
| | 4 | 66 | 0.5005475556 | 0.5005475556 |
| | 6 | 162 | 0.5000886191 | 0.5000886191 |
| | 12 | 322 | 0.5000221913 | 0.5000221913 |
| (iii) QT | A | 12 | 0.5433312606 | 0.4870735087 |
| | B | 18 | 0.5063008435 | 0.5063008435 |
| | C | 34 | 0.5014328795 | 0.5014328795 |
| (iv) asym. | 3n | 66 | 0.4999931111 | 0.4999919721 |
| | 3n | 98 | 0.4999985473 | 0.4999985473 |
| | 3n | 130 | 0.4999995247 | 0.4999995247 |
| | 5n | 42 | 0.5009582361 | 0.5005557772 |
| | 5n | 68 | 0.5000018223 | 0.5000017606 |
| | 5n | 106 | 0.5000003899 | 0.5000002149 |
| (v) hi-fi | | 578 | 0.4999999999 | 0.5000000000 |

Table 2: Convergence of gSIFs to high-fidelity solution.

| Method | | $K_I$ | error [-] | error [%] |
|---|---|---|---|---|
| (iii) QT | A | 18.8248269915 | 3.4427 | 22.38 |
| | B | 17.1446993257 | 1.7626 | 11.46 |
| | C | 15.7671965544 | 0.3851 | 2.50 |
| (iv) asym. | A | 15.7149404150 | 0.3328 | 2.16 |
| | B | 15.6299451660 | 0.2478 | 1.61 |
| | C | 15.4576076163 | 0.0755 | 0.49 |
| (v) hi-fi | | 15.3821134836 | - | - |

Therein, the SBFEM based method variants (ii-iv) are considered. For the case of the established QT crack propagation method (ii), the study was performed based on the amount of refinement around the cracked element for {2,4,6,12} linear elements per long side of the cracked domain. The asymptotic behaviour (iv) of the newly proposed method was studied by

3- and 5-noded elements, denoted by 3n and 5n respectively. Accordingly, the newly proposed asymptotic approach evaluates the mode I SIF employing the same amount of nodes as the QT meshes (Fig. 7), yet with substantially improved accuracy (Tab. 2).

## 4.2 Notched perforated plate

A perforated plate as depicted in Fig. 9 is considered. A notch of length $A = 1$ [mm] is introduced at a distance $L = 18$ [mm] from the bottom right corner. Displacements are prescribed on both sides such that $[u_x, u_y] = [\pm 0.1, 0]$. The material properties are $E = 200$ [N/mm$^2$], $v = 0.3$, $K_{Ic} = 1500$ [N/mm$^{3/2}$]. The height and width of the perforated plate are $H = 24$ [mm] and $W = 60$ [mm] respectively. Plane stress conditions are assumed.
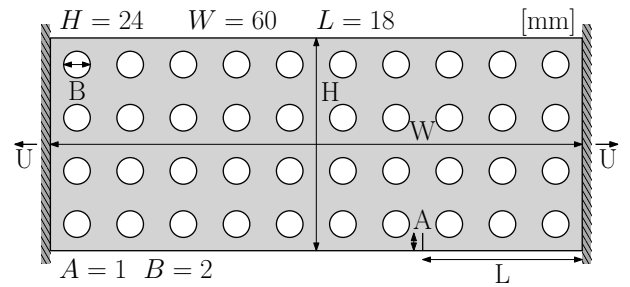


Figure 9: Experimental setup for numerical example 2.

Fig. 10 depicts various snapshots of the various crack propagation phases. During phase 1, the initial discretization is employed, i.e., a fine mesh (green) immediately surrounding the crack front (orange), encased by CM8 and CM16 homogenized elements (red) and tied together by penalty method along the interface (blue). While the conventional SBFEM requires approx. 52'000 DOF, the scaled boundary multiscale approach (MSBFEM) employs 2268 DOF, reducing the amount of DOF by a factor of 22, without perceivable altering the crack path (Fig. 11). Once the crack tip falls within a user specified distance to the adjacent CMX elements, here chosen as one fifth of a CM8 element side length, these are fully resolved as well, resulting in phase 2 (Fig. 10). Analysis by conventional SBFEM results in approx. 58'000

DOF, while MSBFEM employs 4318 DOF, a reduction by a factor of 13. However, the crack paths calculated by the two methods starts to deviate slightly. This is the effect of the linearized boundary conditions, which result from the method with which the multiscale NBF are computed, prescribed on the fully resolved region (green). The imposed linear boundary conditions artificially over-constrain the unit cell, resulting a in stiffer response on the coarse scale, thus impacting the accuracy of the calculated stress field on the fine scale.
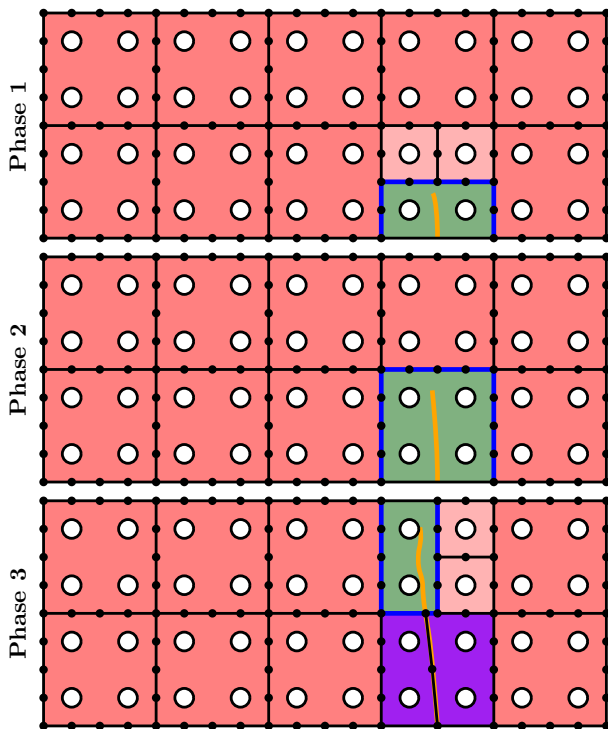


Figure 10: Crack propagation phases 1-3.

In phase 3 (Fig. 10) the crack has transitioned all fully resolved blocks from phase 2. Hence, this region can be replaced by corresponding CMX elements (purple) without incurring a loss in accuracy. To this end, the crack path is smoothed into linear segments joined by the CMX coarse nodes. The computational effort expended in constructing these CMX (purple) elements online is expected to be recuperated over few subsequent crack propagation steps. Indeed, while SBFEM requires approx. 65'000 DOF for analysis, the proposed MSBFEM scheme makes due with 2436 DOF, a reduction by a factor of 26. If the online phase

where to be forgone, the MSBFEM approach would require 6386 DOF and only result in a reduction by a factor of 10. The crack paths do continue to diverge slightly with the effects becoming more visible. First, small deviations are compounded across all crack propagation steps. Second, linearized boundary conditions in the narrow, fully resolved band (phase 3, green) affect the stress state to a greater degree than in the previous phases. By inspection of the two crack paths it seems as if the MSBFEM approach is more resistant to local stress concentrations influencing the gSIFs and thus the crack path incorporates fewer sharp changes in direction as seen in points A, B and C in Fig. 11.
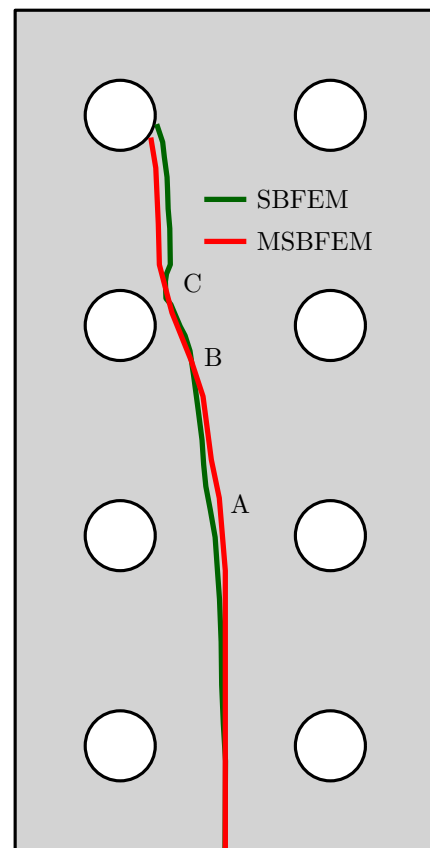


Figure 11: Crack paths for SBFEM and MSBFEM inside the affected subdomain.

## 5 CONCLUSION

MSBFEM is an effective scheme to focus the computational burden of crack propagation analysis on select regions. This is achieved by substituting regions characterized by weak interaction with coarse elements con-

structed by EMsFEM. To this end, the amount of DOF present is reduced by more than an order of magnitude as demonstrated by the crack propagation analysis of a notched, perforated plate. Further, exploiting SBFEM's unique feature set to enhance the quality of calculated gSIFs in post-processing is shown to further reduce the required number of DOFs for standard crack propagation analysis in the fully resolved region. This reduction in the set of active DOFs does not hinder accuracy; the resulting MSBFEM crack path closely resembles the SBFEM reference case.

## Acknowledgements

## REFERENCES

[1] R. Bouc. Forced vibration of mechanical systems with hysteresis. In *Proceedings of the fourth conference on non-linear oscillation*, Prague, Czechoslovakia, 1967.

[2] X. Chen, T. Luo, E. Ooi, E. Ooi, and C. Song. A quadtree-polygon-based scaled boundary finite element method for crack propagation modeling in functionally graded materials. *Theoretical and Applied Fracture Mechanics*, 94:120–133, apr 2018.

[3] S. R. Chidgzey and A. J. Deeks. Determination of coefficients of crack tip asymptotic fields using the scaled boundary finite element method. *Engineering Fracture Mechanics*, 72(13):2019–2036, sep 2005.

[4] G. Dasgupta. A Finite Element Formulation for Unbounded Homogeneous Continua. *Journal of Applied Mechanics*, 49(1):136–140, mar 1982.

[5] A. J. Deeks and J. P. Wolf. A virtual work derivation of the scaled boundary finite-element method for elastostatics. *Computational Mechanics*, 28(6):489–504, jun 2002.

[6] Y. Efendiev and T. Hou. *Multiscale Finite Element Methods*. Springer New York, New York, NY, 2009.

[7] A. W. Egger, E. N. Chatzi, and S. P. Triantafyllou. An enhanced scaled boundary finite element method for linear elastic fracture. *Archive of Applied Mechanics*, 87(10):1667–1706, oct 2017.

[8] T. Y. Hou and X.-H. Wu. A Multiscale Finite Element Method for Elliptic Problems in Composite Materials and Porous Media. *Journal of Computational Physics*, 134(1):169–189, June 1997.

[9] Z. Hu, G. Lin, Y. Wang, and J. Liu. A Hamiltonian-based derivation of Scaled Boundary Finite Element Method for elasticity problems. *IOP Conference Series: Materials Science and Engineering*, 10:012213, jun 2010.

[10] N. Moës, J. Dolbow, and T. Belytschko. A finite element method for crack growth without remeshing. *International Journal for Numerical Methods in Engineering*, 46(1):131–150, Sept. 1999.

[11] A. Müller, J. Wenck, S. Goswami, J. Lindemann, J. Hohe, and W. Becker. The boundary finite element method for predicting directions of cracks emerging from notches at bimaterial junctions. *Engineering Fracture Mechanics*, 72(3):373–386, feb 2005.

[12] E. Ooi, H. Man, S. Natarajan, and C. Song. Adaptation of quadtree meshes in the scaled boundary finite element method for crack propagation modelling. *Engineering Fracture Mechanics*, 144:101–117, aug 2015.

[13] E. Ooi and Z. Yang. Modelling multiple cohesive crack propagation using a finite element–scaled boundary finite element coupled method. *Engineering Analysis with Boundary Elements*, 33(7):915–929, jul 2009.

[14] E. T. Ooi, S. Natarajan, C. Song, and E. H. Ooi. Dynamic fracture simulations using the scaled boundary finite element method on hybrid polygon–quadtree meshes. *International Journal of Impact Engineering*, 90:154–164, apr 2016.

[15] E. T. Ooi, S. Natarajan, C. Song, and E. H. Ooi. Crack propagation modelling in concrete using the scaled boundary finite element method with hybrid polygon–quadtree meshes. *International Journal of Fracture*, 203(1-2):135–157, jan 2017.

[16] E. T. Ooi, C. Song, F. Tin-Loi, and Z. Yang. Polygon scaled boundary finite elements for crack propagation modelling: SCALED BOUNDARY POLYGON FINITE ELEMENTS FOR CRACK PROPAGATION. *International Journal for Numerical Methods in Engineering*, 91(3):319–342, jul 2012.

[17] E. T. Ooi and Z. J. Yang. Modelling crack propagation in reinforced concrete using a hybrid finite element–scaled boundary finite element method. *Engineering Fracture Mechanics*, 78(2):252–273, jan 2011.

[18] E. T. Ooi and Z. J. Yang. Modelling dynamic crack propagation using the scaled boundary finite element method. *International Journal for Numerical Methods in Engineering*, 88(4):329–349, oct 2011.

[19] E. T. Ooi, Z. J. Yang, and Z. Y. Guo. Dynamic cohesive crack propagation modelling using the scaled boundary finite element method: DYNAMIC COHESIVE CRACK PROPAGATION MODELLING. *Fatigue & Fracture of Engineering Materials & Structures*, 35(8):786–800, aug 2012.

[20] G. C. Sih. Strain-energy-density factor applied to mixed mode crack problems. *International Journal of Fracture*, 10(3):305–321, Sept. 1974.

[21] P. Silvester, D. Lowther, C. Carpenter, and E. Wyatt. Exterior finite elements for 2-dimensional field problems with open boundaries. *Proceedings of the Institution of Electrical Engineers*, 124(12):1267, 1977.

[22] C. Song. A matrix function solution for the scaled boundary finite-element equation in statics. *Computer Methods in Applied Mechanics and Engineering*, 193(23-26):2325–2356, jun 2004.

[23] C. Song. A super-element for crack analysis in the time domain. *International Journal for Numerical Methods in Engineering*, 61(8):1332–1357, oct 2004.

[24] C. Song. Evaluation of power-logarithmic singularities, T-stresses and higher order terms of in-plane singular stress fields at cracks and multi-material corners. *Engineering Fracture Mechanics*, 72(10):1498–1530, jul 2005.

[25] C. Song. *The scaled boundary finite element method: intorduction to theory and implementation*. John Wiley & Sons, Hoboken, New Jersey, 2018.

[26] C. Song, F. Tin-Loi, and W. Gao. A definition and evaluation procedure of generalized stress intensity factors at cracks and multi-material wedges. *Engineering Fracture Mechanics*, 77(12):2316–2336, aug 2010.

[27] C. Song and J. P. Wolf. The scaled boundary finite-element method—alias consistent infinitesimal finite-element cell method—for elastodynamics. *Computer Methods in Applied Mechanics and Engineering*, 147(3-4):329–355, aug 1997.

[28] C. Talischi, G. H. Paulino, A. Pereira, and I. F. M. Menezes. PolyMesher: a general-purpose mesh generator for polygonal elements written in Matlab. *Structural and Multidisciplinary Optimization*, 45(3):309–328, mar 2012.

[29] S. P. Triantafyllou and E. N. Chatzi. A hysteretic multiscale formulation for nonlinear dynamic analysis of composite materials. *Computational Mechanics*, 54(3):763–787, Sept. 2014.

[30] S. P. Triantafyllou and E. N. Chatzi. A hysteretic multiscale formulation for validating computational models of heterogeneous structures. *The Journal of Strain Analysis for Engineering Design*, 51(1):46–62, Jan. 2016.

[31] S. P. Triantafyllou and V. K. Koumousis. Hysteretic Finite Elements for the Nonlinear Static and Dynamic Analysis of Structures. *Journal of Engineering Mechanics*, 140(6):04014025, June 2014.

[32] J. P. Wolf. *The scaled boundary finite element method*. J. Wiley, Chichester, West Sussex, England ; Hoboken, NJ, USA, 2003.

[33] J. P. Wolf and C. Song. Consistent infinitesimal finite-element cell method: in-plane motion. *Computer Methods in Applied Mechanics and Engineering*, 123(1-4):355–370, jun 1995.

[34] J. P. Wolf and C. Song. *Finite-element modelling of unbounded media*. Wiley, Chichester, England ; New York, 1996.

[35] Z. Yang. Fully automatic modelling of mixed-mode crack propagation using scaled boundary finite element method. *Engineering Fracture Mechanics*, 73(12):1711–1731, aug 2006.

[36] Z. Yang and A. Deeks. Fully-automatic modelling of cohesive crack growth using a finite element–scaled boundary finite element coupled method. *Engineering Fracture Mechanics*, 74(16):2547–2573, nov 2007.

[37] Z. J. Yang and A. J. Deeks. Modelling cohesive crack growth using a two-step finite element-scaled boundary finite element coupled method. *International Journal of Fracture*, 143(4):333–354, jun 2007.

[38] H. Zhang, Z. Fu, and J. Wu. Coupling multiscale finite element method for consolidation analysis of heterogeneous saturated porous media. *Advances in Water Resources*, 32(2):268–279, Feb. 2009.

[39] H. W. Zhang, J. K. Wu, and Z. D. Fu. Extended multiscale finite element method for elasto-plastic analysis of 2d periodic lattice truss materials. *Computational Mechanics*, 45(6):623–635, May 2010.

[40] H.-W. Zhang, J.-K. Wu, J. Lü, and Z.-D. Fu. Extended multiscale finite element method for mechanical analysis of heterogeneous materials. *Acta Mechanica Sinica*, 26(6):899–920, Dec. 2010.